Supporting Information (SI) for

Production of Nanochitins toward the Shell Biorefinery for Self-assembly Applications as Photonic Film and Pickering Emulsion

Xuhai Zhu[a,§], Fuyan Peng[a,b,§], Hui Li[c], Rongjun Lin[a,b], Rui Lu[a], Fang Lu[a,*]

[a]Dalian Institute of Chemical Physics, Chinese Academy of Sciences,116023, Dalian, China.

[b]Henan Institute of advanced technology, Zhengzhou University, 450052, Zhengzhou, China.

[c]Zhengzhou Tobacco Research Institute, China National Tobacco Corporation, Zhengzhou, 450001, China.

[§]Authors are equally contributed to this work.

*Corresponding author, Fang Lu–E-mail: lufang@dicp.ac.cn / Mailing address: Dalian Institute of Chemical Physics, CAS, 457 Zhongshan Road, 116023, Dalian, China / Tel.: +86–0411-8437-9846.

Table of Contents

1. EXPERIMENTAL METHODS

1.1 Materials

All chemicals and solvents were analytical grade and purchased from Sinopharm Chemical Reagent Co., Ltd (Shanghai, China) or Aladdin Reagent Co., Ltd. (Shanghai, China) if otherwise stated. Fresh shrimps (Penaeus chinensis), crawfish (Procambarus clarkii), and crabs (Portunus trituberculatus) used in the experiments were acquired in the Malai market of Dalian, China. They were cooked, and the meat was consumed while the residual shells were collected, washed, and dried. The contents of chitin, minerals (dominantly $CaCO_3$), and protein in crustacean shells were quantified according to the reported method.[1] Milli-Q water with a resistivity of 18.2 MΩ.cm (at 25 °C) was used in our experiment. Dialysis membrane (MD77), with a molecular weight cutoff of 14,000, was purchased from Beijing Henghui Technology Co., Ltd., China.

1.2 Self-assembly of NCh induced by water-evaporation

ChNC solid film. ChNC dry film was obtained by the conventional solution-casting method: 10 mL of 5wt% ChNC suspension was processed with sonication for about 10 minutes through an ultrasonic processor, followed by storage in a polystyrene Petri dish (35 mm inner diameter) to slow down evaporation until a dry solid film was formed.

ChSR solid film. ChSR dry film was prepared using the blade-casting method: 8mL of 2wt% ChSR gel was deposited in front of the blade on the glass plate, and the blade moved at a certain speed such that an area was uniformly coated. The blade-coated film was left undisturbed and slowly dried under ambient conditions.

1.3 Characterization

Particle size and zeta potential measurement. To determine the surface charge and suspension stability of the NCh products, their zeta potential and particle size distribution were determined using a Zetasizer Nano ZS90 (Malvern Instrument, UK), which was based on dynamic light scattering (DLC). This is based on Brownian motion: smaller particles move and diffuse faster than larger particles. Since the DLS is based on the assumption that the analyzed particles are spherical, the diameter of equivalent sphere model for our non-spherical particle was measured. Considering the price and easy availability of this technique, we used it to quickly screen our results in the experimental optimization stage. All the samples were diluted to 0.05 wt% and dispersed under ultrasonic treatment for 30 min before measurement. Each sample was measured three times at 25 °C, and the average data was adopted after analyses.

Morphology analysis. The shape and size of NCh products were observed using transmission electron microscopy (TEM, JEM-2100, JEOL Co., Ltd., Japan) at an accelerating voltage of 200 keV. Before the TEM observation, the NCh suspension was diluted to 0.05 wt% by adding anhydrous ethanol and then ultrasonicated for 10 min to get a homogeneous solution. A droplet of the diluted suspensions was deposited and allowed to dry onto the 300-mesh carbon-coated copper grid. The morphologies of the NCh products were further observed by an atomic force microscope (AFM, SPM-9700, SHIMADAZU Co., Ltd., Japan) in tapping mode using a standard silicon cantilever. A few drops of NCh aqueous suspension (0.005 wt%) were deposited onto mica discs (12 mm), after which water evaporated. Scanning was conducted using the NanoWorld® Pointprobe® NCH probe, with a 1Hz scan rate and 256×256-pixel image resolution. Image processing and section analysis were performed with ImageJ software (1.54f, Java 1.8.0_322).

The microstructure of ChNC-based films was revealed using a scanning electron microscope (SEM, JSM-7800F, JEOL Co., Ltd., Japan) with an accelerating voltage of 15 kV. The pure ChNC solid film was frozen under liquid nitrogen, then fractured, mounted, coated with Pt on a JEOL JFC-1100E ion sputter coater, and observed. The ChNC/PVA composite film sprayed onto the 0.5×0.5 cm stainless-steel plate was directly loaded in the microscope to observe.

The thickness of the ChNC/PVA composite film was measured by Atomic force microscopy (NanoWizard Ultra Speed &inVia Raman).

To characterize the surface morphology and identify the hetero-aggregates adsorbed at the droplet surface, ChSR-stabilized styrene (St)-in water Pickering emulsions were prepared as described in the previous method.[2] The dried polystyrene (PS) beads were metalized with Pt and visualized with the JEOL JSM-7800F instrument under an accelerated voltage of 15 kV.

X-ray diffraction analysis. Freeze-dried chitin and NCh samples were ground evenly and laid flat in the glass grooves. The phase structure of samples was then analyzed by an X-ray powder diffractometer (XRD, Empyrean-100, PANalytical B.V., Netherland) equipped with a Cu, Kα radiation source (λ = 1.5418 Å) operating at 40 kV. 2θ scans were performed from 5° to 60° with a 4°/min speed. The crystallinity index (CrI) was calculated based on Segal's method (Eq. 1):

$$\mathrm{CrI} = \frac{I_{110} - I_{AM}}{I_{110}} \times 100\% \qquad (1)$$

where I_{110} is the diffraction intensity for the (110) plane at around 2θ =19° while I_{AM} is the amorphous diffraction intensity at around 2θ = 15°.

FT-IR Spectroscopy. FT-IR spectra of chitin and NCh samples were recorded in the region of 4000−400 cm^{-1} on a Fourier transform infrared spectrometer (Nicolet 6700, Thermo Fisher Scientific, America) using potassium bromide pellets. For testing, the original chitin and corresponding NCh products were dried at 60 °C to eliminate water from the samples. FT-IR in attenuated total reflection (ATR) mode was used.

Solid NMR spectroscopy. The solid-state NMR experiments were performed on a Bruker Avance III 400 NMR spectrometer using a 4 mm WVT probe (Bruker). Magic angle spinning (MAS) frequency of the sample was 14 kHz. Amplitude modulated cross-polarization (CP) with D1=2 was used to obtain ^{13}C CP/MAS NMR spectra. The corresponding ^{1}H and ^{13}C 90° pulse is 3.03 μs and 4.09 μs, respectivly.

The spectra were processed using TopSpin software (Bruker, Version 4.0.7). The spectra processing included a backwards linear prediction of the beginning of the FID, phase correction, baseline adjustion and integration of the CH_3 signal region and the polysaccharidic backbone region (C1–C6). The degree of deacetyltion of chitin and chitosan were calculated from Eq. 2,

$$mol\ (\%) = \frac{I_{CH3}}{(I_{C1} + I_{C2} + I_{C3} + I_{C4} + I_{C5} + I_{C6})/6} \times 100 \qquad (2)$$

where I_{CH3} and (I_{C1}+I_{C2}+I_{C3}+ I_{C4}+ I_{C5}+ I_{C6}) corresponds to the integral of carbon atom in CH_3 of acetyl groups and to the the integral of carbon atom in polysaccharidic backbone.

Thermogravimetric analysis. The thermal properties of chitin and NCh samples were characterized with a thermogravimetric analyzer (TGA, STA 449 F3, Netzsch, Germany). The samples were heated under a nitrogen atmosphere from room temperature to 800 °C at a heating rate of 10 °C/min. The derivative thermogravimetric analysis (DTG) curves were plotted from the TGA data.

Interfacial wettability of ChSR solid film. A three-phase contact angle (CA) was measured by the sessile drop method to characterize the wettability of ChSR at the oil/water and air/water interfaces. The prepared ChSR solid film was transferred to a chamber filled with sunflower oil or air. A water droplet was generated on a syringe tip and moved to the film's surface. After that, the droplet shape was monitored with a digital camera for 2 min. The TCA was reported as the angle at the three-phase line (film, water, and oil /air).

Optical characterization. A polarized optical microscope (POM, GX71, Olympus, Japan) equipped with a CCD camera (Leica DFC295, Germany) was used to detect the chiral nematic phase and characterize the photonic surface of the ChNC/PVA composite film, which was sprayed onto the 1.0×1.0 cm stainless-steel plate. Photographs of the composite films sprayed onto the 10×10 cm stainless-steel plate were taken by a smartphone camera under white light without a polarizer.

Microscopy of emulsion. The microstructure of emulsion samples was examined by a spinning disk confocal microscope with a 20× / NA 0.75 dry objective lens (Revolution WD, Andor Technology Ltd, United Kingdom). 6 μL of diluted samples were placed on a microscope slide and covered with a glass coverslip without squeezing the assembly. The emulsions fabricated in different mass ratios of oil to water and by ChSR with various concentrations were observed under the white light source (cool LED pE-100) to measure the droplet size. The oil phase and ChSR in the emulsions and the type of emulsions were identified with the aid of the LU-NV laser unit (Nikon Instruments Inc.). The procedures for preparing fluorescent labeling emulsions have already been described above. Also, the excitation wavelengths for the Nile red and FITC used in this study were 488 and 543 nm, respectively. An Andor Neo16-bit CMOS camera with a 2560×2160-pixel chip was used to record the confocal images. The resulting images were processed with ImageJ (1.54f, Java 1.8.0_322).

2. EXPERIMENTAL RESULTS

2.1 Dependence of ChNC to ChSR ratio on hydrolysis severity

Table S1. RSM-BBD experimental design matrix and response data.

Run no.	Factors			Experimental yield			
	A, °C	B, h	C, mol	ChNC	ChSR	Total NCh	Carbohydrate losses
1(1)	100	4	0.6	3.53	93.31	96.84	3.16
2(3)	130	2	0.9	40.29	52.98	93.27	6.73
3(3)	115	6	0.6	35.37	56.67	92.04	7.96
4(2)	100	6	0.9	14.31	81.07	95.38	4.62
5(3)	115	4	0.9	37.47	55.04	92.51	7.49
6(1)	100	2	0.9	3.55	93.79	97.34	2.66
7(3)	130	4	0.6	34.31	55.82	90.13	9.87
8(3)	130	6	0.9	37.09	52.02	89.11	10.89
9(2)	100	4	1.2	12.5	83.46	95.96	4.04
10(3)	130	4	1.2	41.45	49.44	90.89	9.11
11(3)	115	2	1.2	31.71	63.92	95.63	4.37
12(3)	115	4	0.9	38.31	55.3	93.61	6.39
13(3)	115	4	0.9	38.55	55.97	94.52	5.48
14(3)	115	4	0.9	41.21	49.52	90.73	9.27
15(2)	115	2	0.6	18.65	74.75	93.40	6.60
16(3)	115	6	1.2	39.44	51.94	91.38	8.62
17(3)	115	4	0.9	39.67	54.51	94.18	5.82

The experimental design matrix and the responses based on 17 experimental runs conducted in our study are given in Table S1. Depending on the severity of reaction conditions, ChNC yields varied between 4% and 41%, and ChSR yields ranged between 49% and 94%. The cluster analysis technique was then used to condense the yield data into smaller, more coherent groups, where each group represents similar yields. The data were first standardized, and the k-means clustering approach was used to identify the optimal number of clusters for appropriate data classification (Figure S1A). Cluster 1 consisted of two runs (1, 6), characterized by very high ChSR yields (93–94%), meager ChNC yields (< 4%), and negligible carbohydrate losses (< 4%) (Figure S1A & Table S1). ChSR recovered in these runs was not furtherly hydrolyzed into the ChNC, which could be attributed to the low reaction temperature (100 °C). These conditions were favorable for hydrolyzing the chitin just enough to get the ChSR products without substantial conversion into

ChNC and/or degradation into sugars. If the goal is to produce ChSR, the conditions of run 6, i.e., n(acid)/n(GlcNAc) = 0.9, 100 °C and 2 h, will be more suitable because of high yields obtained with a conservative use of acid and energy (lower temperature and less time). Cluster 2 consisted of three runs (4, 9, and 15) with relatively more ChSR than ChNC yields and minimal losses ranging between 4 and 7% (Figure S1A & Table S1). Cluster 3 consists of twelve runs (2, 3, 5, 7, 8, 10, 11, 12, 13, 14, 16, and 17), in which cellulose lost in the waste stream ranged between 4–11% and total NCh yield ranged between 89 and 96% (Figure S1A & Table S1). It can be observed that the gap between ChSR and ChNC yields was reduced with the increase in reaction severity. It is reasonable that the hydrolysis of ChSR into ChNC increased. Moreover, it seems that the dominant effect of temperature in chitin depolymerization kinetics, as evident from runs 2 and 10, with the highest CNC yields (~41%) in this cluster. Therefore, the potential for maximizing ChNC yields from purified chitin lies in optimizing around the parameters of n(acid)/n(GlcNAc) = 0.9–1.2, 115–130 °C, and 2–6 h. Specific hydrolysis process conditions were found to facilitate the production of NCh of different types in high yields.

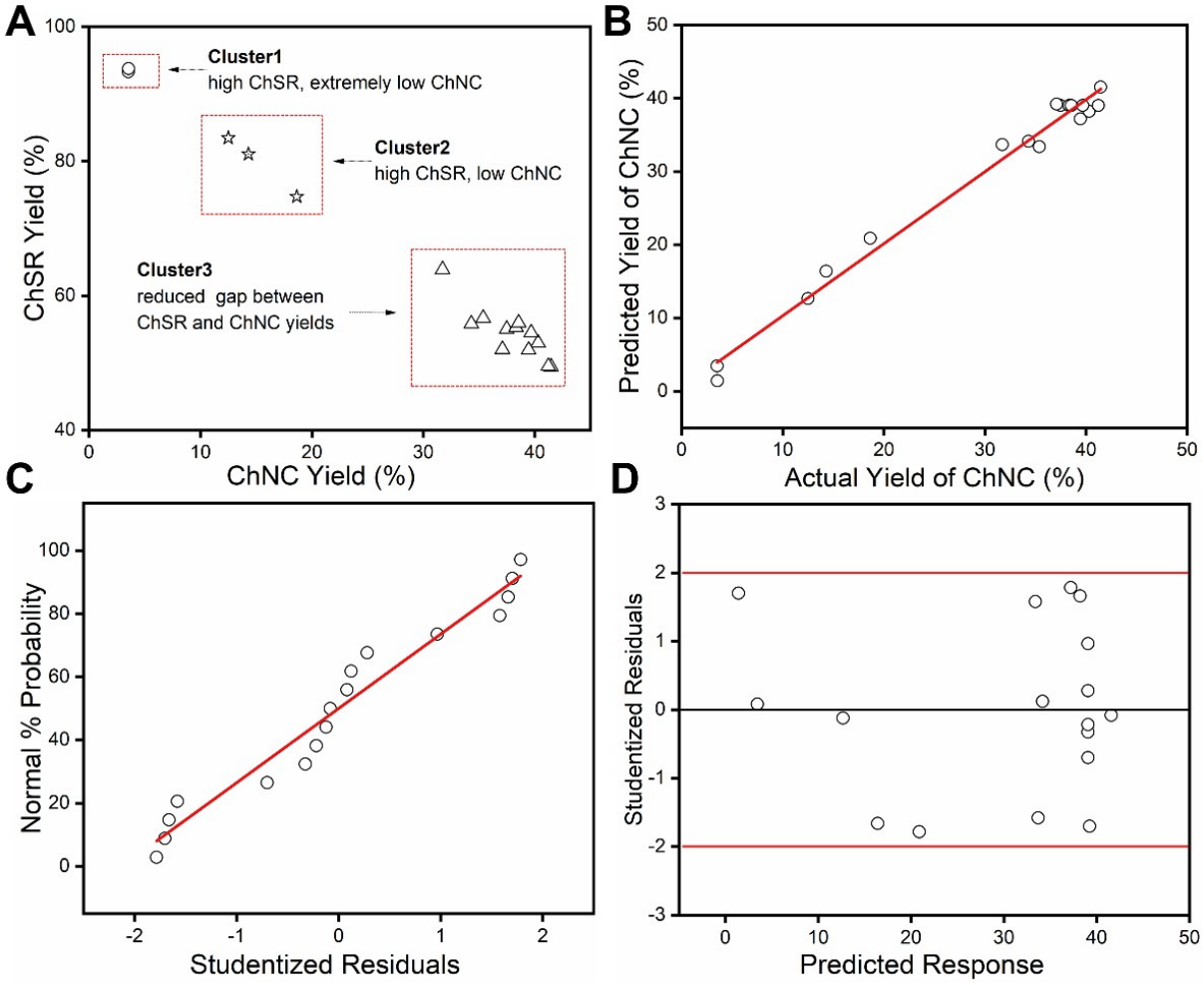

Figure S1. Diagnostic plots of optimization process using central composite design; cluster analysis of experimental ChNC and ChSR yields (A), plot of predicted versus actual ChNC yield (B), normal probability plot of the studentized residuals (C), plot of the studentized residuals versus predicted response.

2.2 Model fitting and statistical analysis

Table S2. ANOVA for response surface quadratic model of ChNC production yield.

Source	Sum of Squares	Mean Square	F-value	P-value(Pro＞F)	
Model	2880.82	320.09	50.76	＜0.0001	Significant
A-Temperature	1777.57	1777.57	281.91	＜0.0001	
B-Time	128.08	128.08	20.31	0.0028	
C-Acid content	138.11	138.11	21.90	0.0023	
AB	48.72	48.72	7.73	0.0273	
AC	0.84	0.84	0.13	0.7263	
BC	20.21	20.21	3.2	0.1166	
A^2	585.13	585.13	92.80	＜0.0001	
B^2	49.93	49.93	7.92	0.0260	
C^2	78.07	78.07	12.38	0.0097	
Residul	35.79	11.93			
Lack of Fit	8.34	2.09	5.72	0.0626	Insignificant
Standard deviation		2.51			
Mean		29.85	R^2		0.9849
C.V.%		8.41	Adjusted R^2		0.9655
Adequate precision		20.842	Predicted R^2		0.7997

The second-order polynomial model that correlates the yield of ChNC to the three independent process variables was obtained (Eq. 3):

$$Y = 13.60A + 25.64B + 126.65C - 0.12AB - 0.10AC - 3.75BC - 0.05A^2 - 0.86B^2 - 47.84C^2 - 918.66 \quad (3)$$

where Y is the yield of ChNC; A, B, and C are the reaction temperature, reaction time, and molar ratio of acid to GlcNAc, respectively. The reaction model suggests a positive effect of A, B, and C on increasing the ChNC yield. However, all the quadratic terms negatively affected decreasing the ChNC yield. It is reasonable that the synergy of two variables could lead to excessive hydrolysis of ChNC into water-soluble sugars or other by-products, resulting in a low yield of ChNC. The analysis of variance (ANOVA) for the fitted quadratic polynomial model is presented in Table S2. It is indicated that the investigated process parameters significantly affect the yield of ChNC, as implied by the model F-value of 50.76, and the p-value of the model is less than 0.0001. Insignificance of the "lack of fit" test (p-value of 0.0626) confirms the model's suitability in this experiment. The determination coefficient (R_2 = 0.9849) is close to 1, proving that the regression model explained the system's true behavior well.[3] This also can explain why most of the data points on the predicted versus actual ChNC yield plot lie close to the experimental values, as shown in Figure S1B. The normal probability plot specifies that the normal% probability distribution follows the residuals. These data points in the plots are fitted to the straight line in Figure S1C, suggesting the quadratic polynomial model satisfies the analysis of the assumptions of variance.[4] Figure S1D also explains that the difference of studentized residuals versus predicted has no individual form.[5] As a result, it may be inferred that the obtained residuals have the expected

scattering and that the proposed model is adequate. Therefore, all these statistical tests show that the quadratic models developed are qualified to represent the correlation between the response and the independent process variables.

2.3 NMR results on recycled PTSA

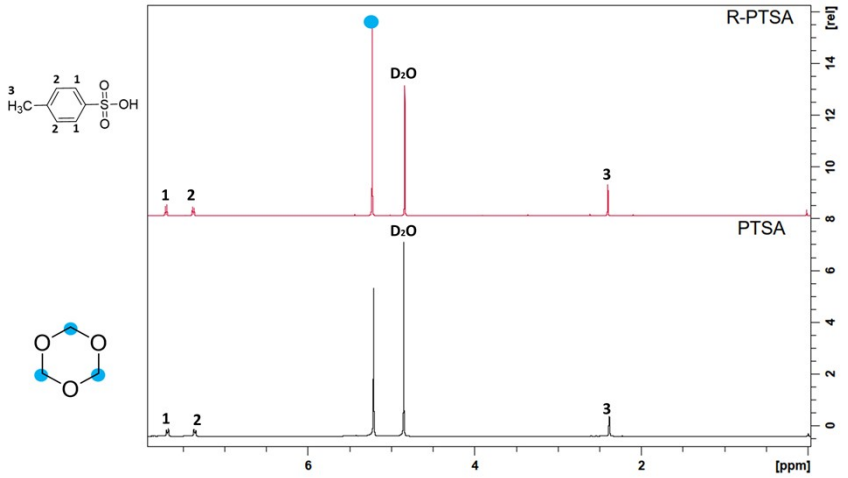

Figure S2. ^{1}H NMR spectra of R-PTSA and PTSA

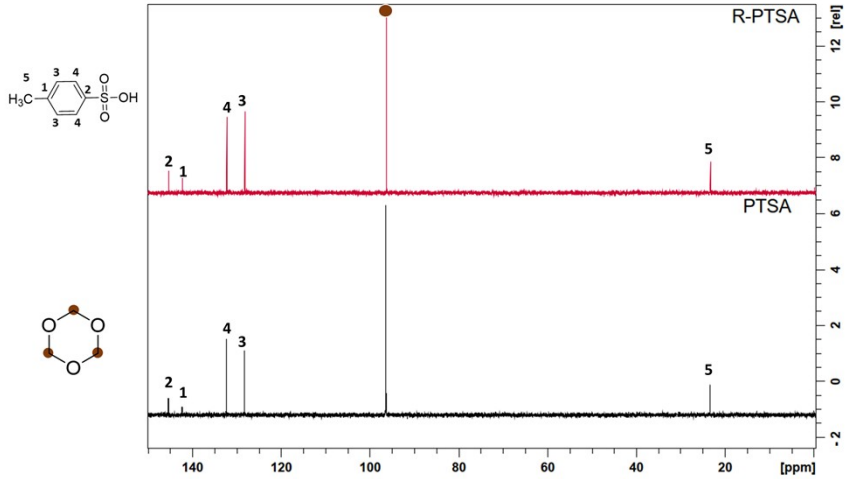

Figure S3. ^{13}C NMR spectra of R-PTSA and PTSA

Table S3. Performance evaluation of acid recovery

	Recovery yield (%)	Purity (%)	ChNC/ChSR Yield (%)	ChNC Z-average size (nm)	ChNC PDI	ChNC Zata-potential (mV)
PTSA	-	91.2%	39.1/53.7	81	0.23	+41.5
R-PTSA	79.5%	89.8%	32.7/58.9	81.6	0.25	+38.4

2.4 NMR results on NCh products

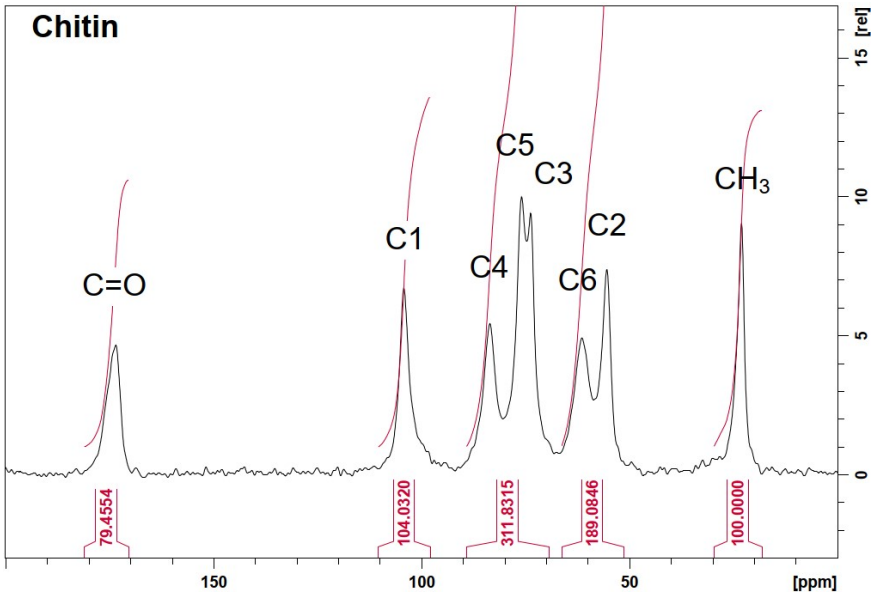

Figure S4. ^{13}C solid-NMR spectra of purified chitin

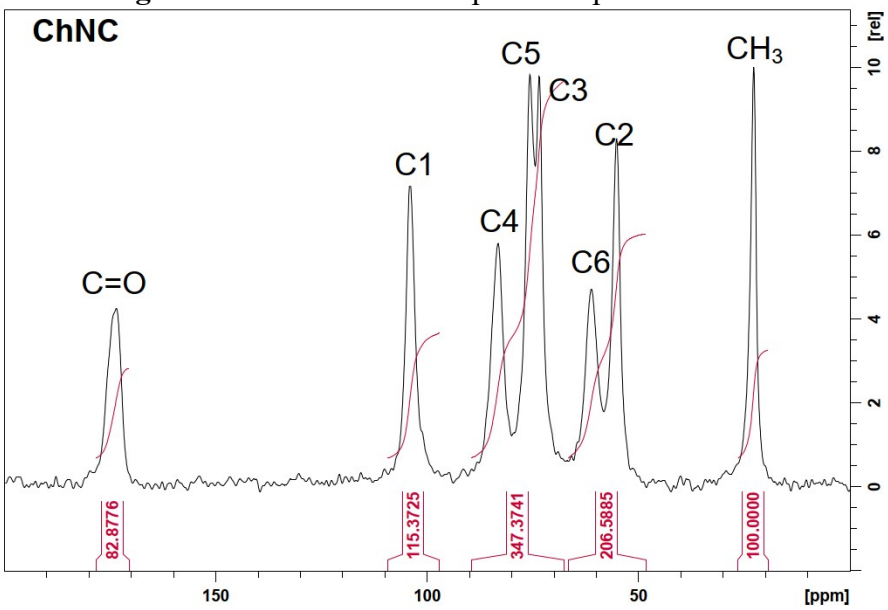

Figure S5. ^{13}C solid-NMR spectra of ChNC product

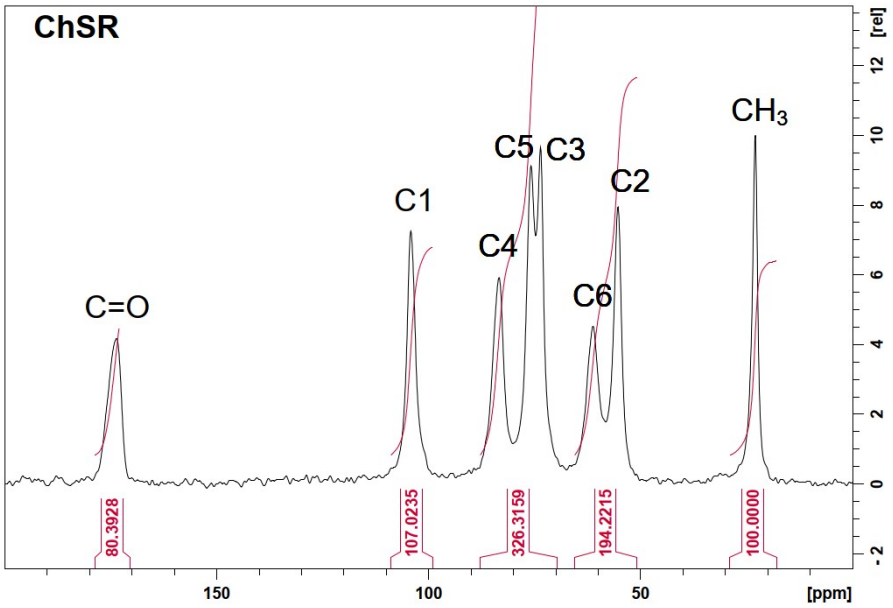

Figure S6. ^{13}C solid-NMR spectra of ChSR product

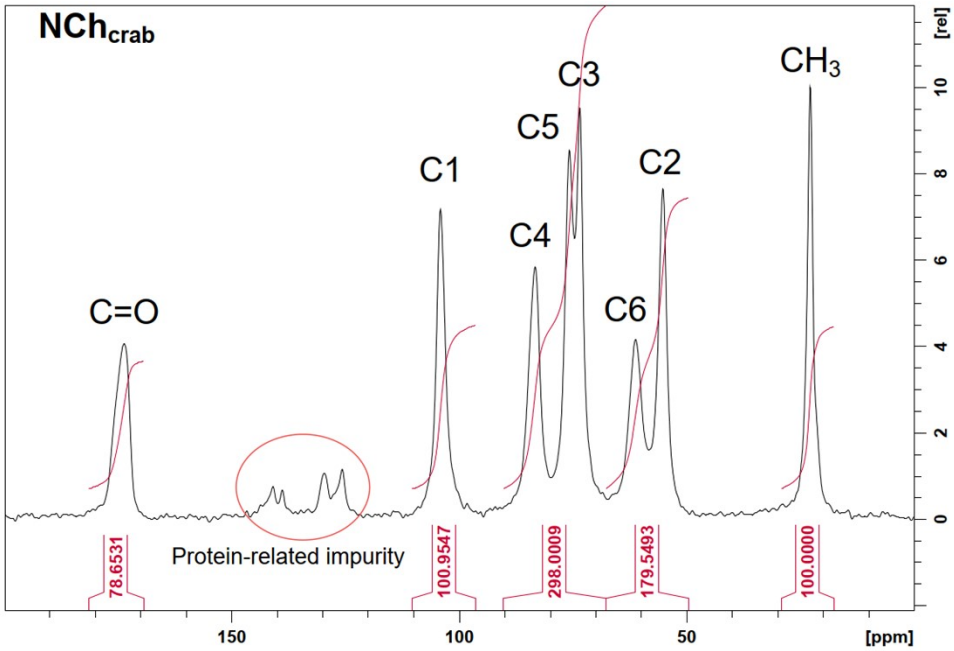

Figure S7. ^{13}C solid-NMR spectra of NCh_{crab} product

2.5 Optimal results on the application of NChs

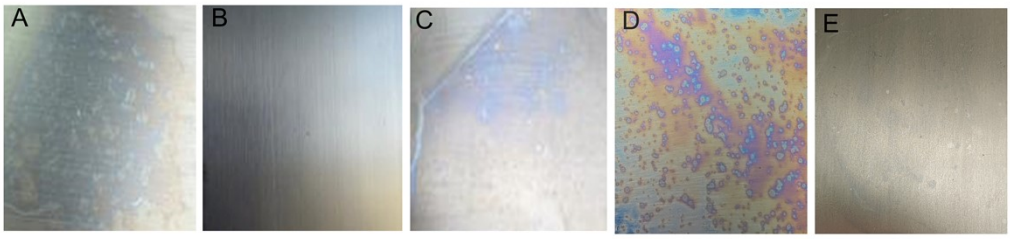

Figure S8. Optimization of photonic film preparation conditions, (A) 0.5 wt% ChNC, (B) 0.5 wt% ChNC and 5 wt%PVA, (C) 1 wt% ChNC, (D) 1 wt% ChNC and 0.5 wt% PVA, (E) 1 wt% ChNC and 2 wt% PVA

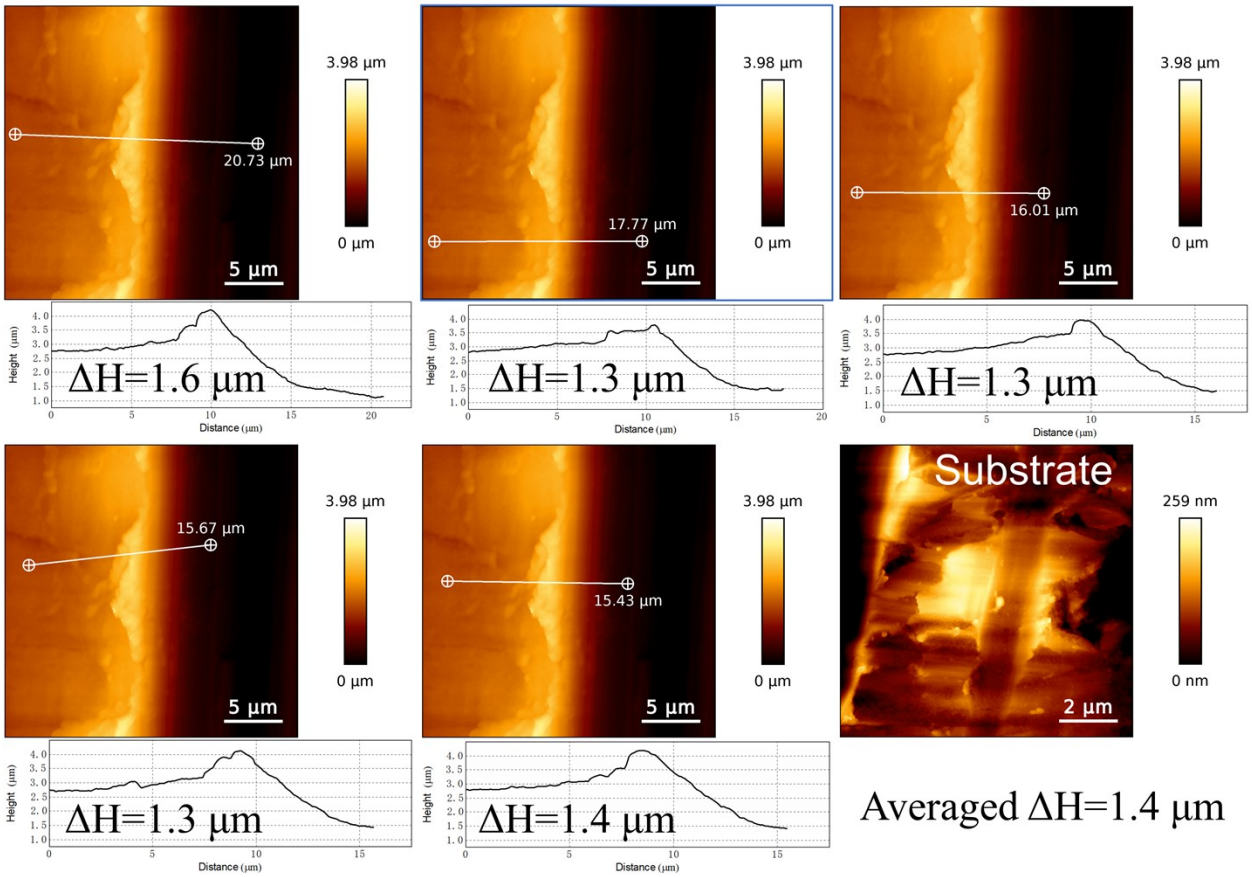

Figure S9. AFM plane morphology of photonic film at five different points, and the bottom height vs. distance image corresponding the above white profile.

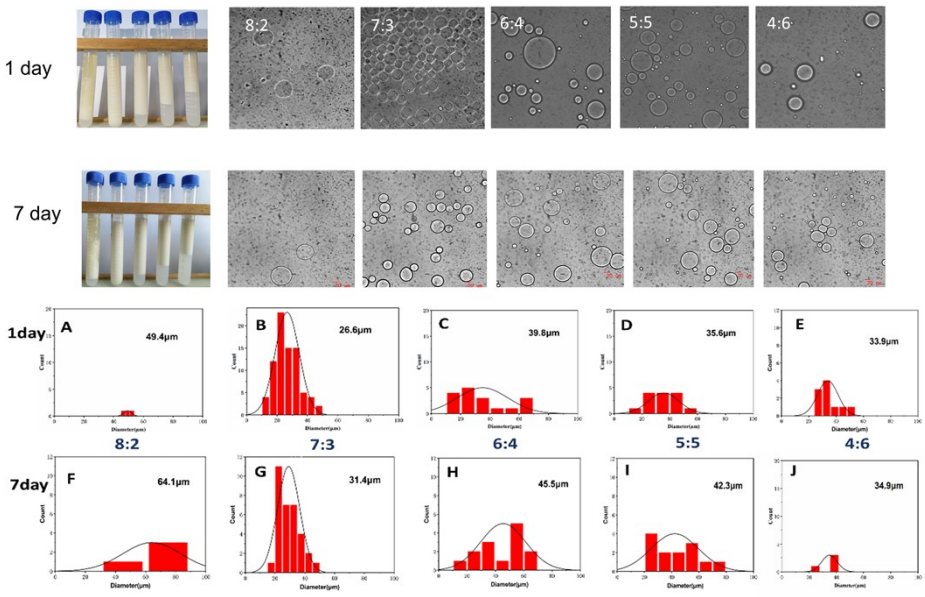

Figure S10. The effect of oil to water mass ratio on the stability and particle size of emulsion droplets.

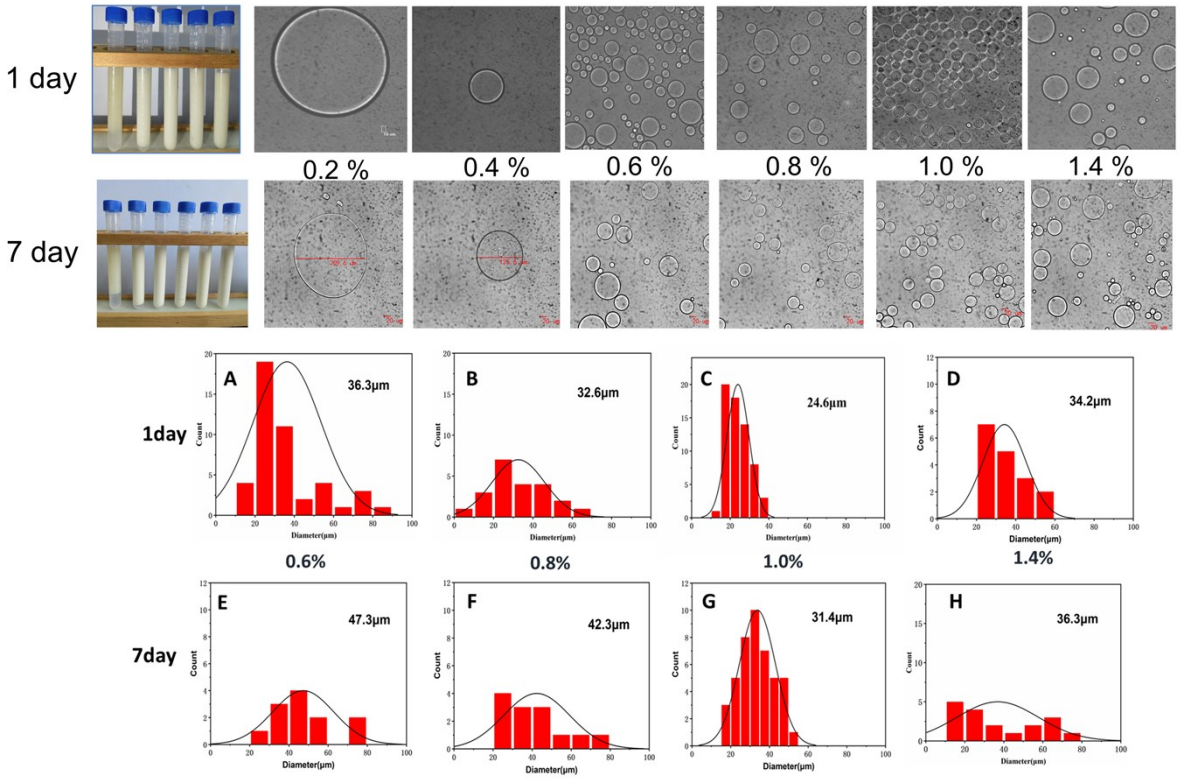

Figure S11. The effect of ChSR concentration on the stability and particle size of emulsion droplets.

3. REFERENCES

[1] F. Shahidi, J. Synowiecki, *J. Agric. Food Chem.* **1991**, *39*, 1527.

[2] I. Kalashnikova, H. Bizot, B. Cathala, I. Capron, *Biomacromolecules* **2012**, *13*, 267.

[3] E. G. Bacha, *S. Afr. J. Chem. Eng.* **2022**, *40*, 176.

[4] G. Kandhola, A. Djioleu, K. Rajan, N. Labbé, J. Sakon, D. J. Carrier, J. W. Kim, *Bioresour. Bioprocess.* **2020**, *7*, 1.

[5] Khushbu, R. Jindal, *J. Appl. Polym. Sci.* **2022**, *139*, e52706.